

Phase-ordering kinetics on graphs

R. Burioni,¹ D. Cassi,¹ F. Corberi,² and A. Vezzani³

¹Dipartimento di Fisica and INFN, Università di Parma, Parco Area delle Scienze 7/A, I-423100 Parma, Italy

²Dipartimento di Fisica “E.R.Caianiello” and CNR-INFM, Università di Salerno, 84081 Baronissi (Salerno), Italy

³Dipartimento di Fisica and CNR-INFM, Università di Parma, Parco Area delle Scienze 7/A, I-423100 Parma, Italy

(Received 19 July 2006; published 17 January 2007)

We study numerically the phase-ordering kinetics following a temperature quench of the Ising model with single spin-flip dynamics on a class of graphs, including geometrical fractals and random fractals, such as the percolation cluster. For each structure we discuss the scaling properties and compute the dynamical exponents. We show that the exponent a_χ for the integrated response function, at variance with all the other exponents, is independent of temperature and of the presence of pinning. This universal character suggests a strict relation between a_χ and the topological properties of the networks, in analogy to what is observed on regular lattices.

DOI: 10.1103/PhysRevE.75.011113

PACS number(s): 64.60.Cn, 05.70.Ln, 89.75.Hc

I. INTRODUCTION

After quenching a system from a high temperature disordered state to an ordered phase with broken ergodicity, a phase-ordering kinetics is observed, characterized by coarsening of quasiequilibrated domains with a typical size $L(t)$. Although a first-principle theory of phase ordering is presently lacking, for systems defined on homogeneous lattices a substantial comprehension of the dynamics has been achieved by means of exact solutions of soluble cases, approximate theories, and numerical simulations [1]. While the inner of domains is basically in equilibrium at the quench temperature, the off-equilibrium behavior is provided by the slow evolution of their boundaries. As a consequence, at each time s , for space separations $r \ll L(s)$ or for time separations $t-s \ll s$ intradomains quasiequilibrium properties are probed, while for $r \gg L(s)$ or $t-s \gg s$ one explores interdomains properties, where the aging behavior is observed. Accordingly, the correlation of the order parameter $\langle \sigma_i(t) \sigma_j(s) \rangle$ between sites i, j at times s, t can be expressed as the sum of two terms

$$\mathcal{C}_{ij}(t,s) = \mathcal{C}_{ij}^{st}(t-s) + \mathcal{C}_{ij}^{ag}(t,s). \quad (1)$$

The first term describes the equilibrium contribution provided by the interior of domains while the second contains the nonequilibrium information. Analogously, also the integrated response function, or zero field cooled magnetization, measured on site i at time t after a perturbation has switched on in j from time s onward, takes an analogous additive form

$$\chi_{ij}(t,s) = \chi_{ij}^{st}(t-s) + \chi_{ij}^{ag}(t,s). \quad (2)$$

On regular lattices, due to space homogeneity and isotropy, correlation and response function depend only on the distance r between i and j . One has, therefore, $\mathcal{C}_{ij}(t,s) = \mathcal{C}(r,t,s)$, and similarly for $\chi_{ij}(t,s)$.

At the heart of the nonequilibrium behavior is the dynamical scaling symmetry, a self-similarity where time acts solely as a length rescaling. When scaling holds, the states sequentially entered by the system are statistically equivalent provided lengths are measured in units of the characteristic size $L(t)$ of ordered domains. All the time dependence must

enter through $L(t)$, and the aging parts in Eqs. (1) and (2) take a scaling form in terms of rescaled variables [2] $x=r/L(s)$ and $w=L(t)/L(s)$,

$$\mathcal{C}^{ag}(r,t,s) = \tilde{\mathcal{C}}(x,w), \quad (3)$$

$$\chi^{ag}(r,t,s) = s^{-a_\chi} \tilde{\chi}(x,w). \quad (4)$$

The characteristic length grows according to a power law $L(t) \sim t^{1/z}$. Nonequilibrium exponents such as a_χ, z , are expected to be universal. Namely, they depend only on a restrict set of parameters, such as space dimensionality and number of components \mathcal{N} of the order parameter, on the conservation laws of the dynamics and are independent of temperature.

In defiance of this basic comprehension in homogeneous systems, our understanding of phase ordering on inhomogeneous structures is particularly poor, although examples, ranging from disordered materials, to percolation clusters, glasses, polymers, and biomolecules, may be abundantly found in physics, economics, chemistry, and biology [3].

In this paper we study the phase-ordering kinetics of the Ising model with nonconserved order parameter on some *physical graphs* [4], namely networks with the appropriate topological features to represent real physical structures. These structures are constrained to be embeddable in a finite dimensional space and to have bounded coordination number. Among these, we consider random fractals, i.e., percolation clusters, and geometrical fractals, such as the Sierpinski gasket and carpet and others (see all the cases considered in Fig. 1). We discuss the results of numerical simulations and compare them with the predictions provided by a large- \mathcal{N} model, where exact calculations can be carried out [5,6]. In the large- \mathcal{N} model the general framework of scaling behavior is maintained on generic graphs, and the exponents depend on the topology of the network only through the fractal dimension d_f and the spectral dimension d_s , a large scale parameter encoding the relevant topology. In particular, one finds $z=2d_f/d_s$ and $a_\chi=(d_s-2)/2$. As observed in Ref. [7] and in our simulations, this general framework provided by the soluble model seems to be quite unrepresentative of the situation in scalar systems, with discrete symmetry, e.g., Ising

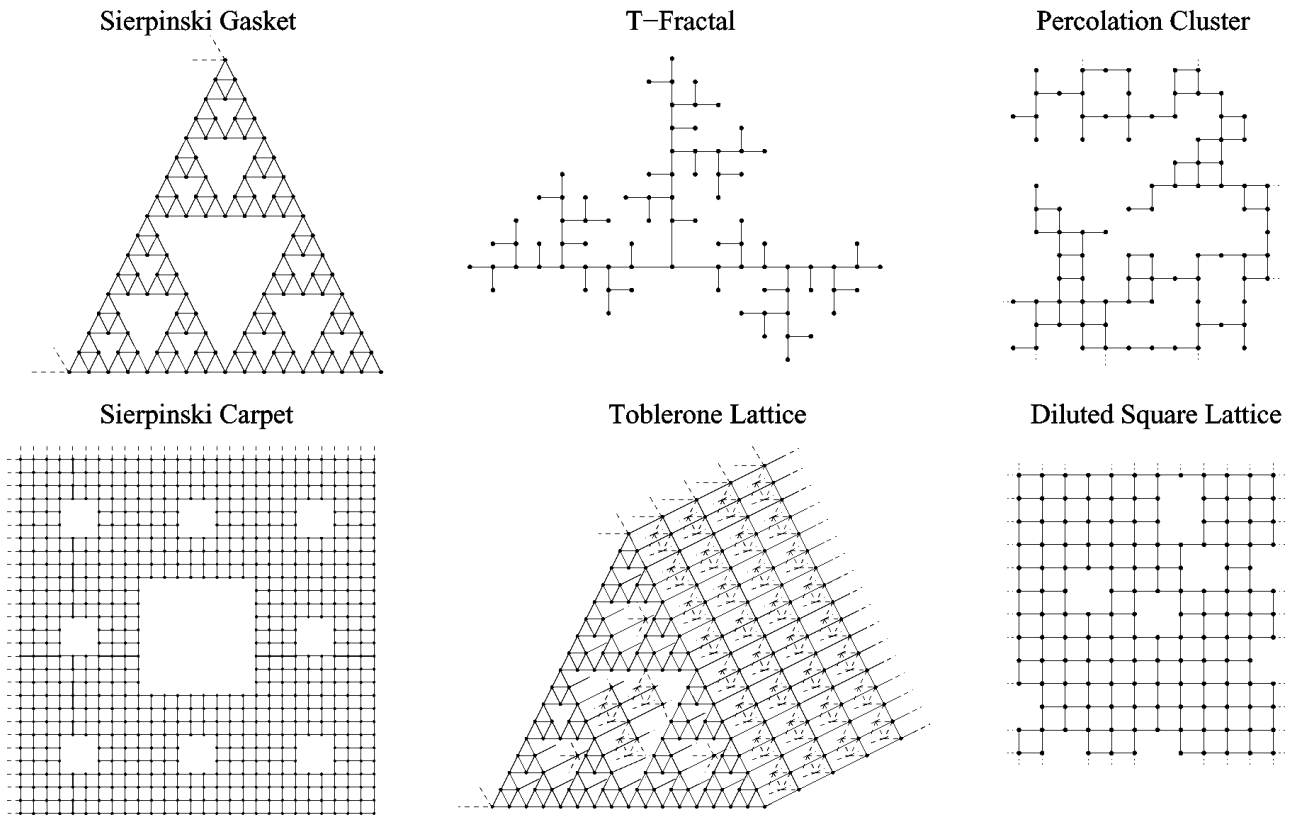


FIG. 1. The structures considered in the paper.

and Potts.. A basic feature missed is the fundamental role played by activated processes on inhomogeneous structures. Actually, on homogeneous structures the temperature is an irrelevant parameter, in the sense of the renormalization group [1]. Long-time, large-scale properties do not depend on the quench temperature in the whole low temperature phase. Exponents related to the aging behavior are then independent of the thermal noise. On the other hand, structure inhomogeneities exert a pinning force on interfaces or other topological defects, whose further evolution can only be mediated by activated processes. Activated processes may be present in nondisordered models on regular lattices as well, where they sometimes play a fundamental role, but without changing large-scale, long-time properties. On fractal sets, on the other hand, pinning forces are exerted on many length scales and contribute to the aging behavior. These forces cause a stop-and-go behavior hindering the power laws and preventing a straightforward definition of the exponents. At relatively high temperatures, where pinning barriers are more easily surmounted, slip-stick effects are less severe. In these cases the general scaling scheme (3) and (4) can be investigated and the nonequilibrium exponents can be defined. It turns out, however, that pinning forces are still subtly at work, making exponents temperature dependent.

A notable exception in this vague scenario is represented by the response function exponent a_χ . Interestingly, at variance with all the other exponents, its value only depends on the structure considered, is independent of temperature and of the presence of stick-slip intermittency. This universal character calls for a strict and direct relation between a_χ and

precise topological properties of the network, bypassing any microscopic dynamical mechanism. We develop an argument showing the relation between this exponent and fundamental equilibrium properties. In particular, a_χ must take a positive value whenever the statistical model on the network considered has a phase transition at a finite critical temperature T_c , whereas $a_\chi=0$ on structures with $T_c=0$. The same picture is provided by the solution of the large- \mathcal{N} model on graphs. This is what we find, with good accuracy, in the simulation of discrete symmetry models on all the inhomogeneous structures considered. We measure $a_\chi=0$ or $a_\chi>0$ whenever structures with $T_c=0$ or $T_c>0$ are considered. This is of particular interest, since for discrete symmetry models, topological and connectivity properties are known to play a fundamental role in determining equilibrium and critical behavior [8], but a direct link with the topological features of the network is still lacking. Our results provide an evidence for some relationship between nonequilibrium kinetics and large scale topology on general networks and suggest that the same topological features of graphs determine critical behavior and nonequilibrium exponent a_χ during phase ordering [6].

This paper is organized as follows: In Sec. II we introduce the Ising model that will be considered in the simulations. We also introduce the basic observables, and discuss the numerical techniques. In Sec. III we discuss the outcome of the numerical simulations on different structures. In particular, Sec. III A deals with structures with $T_c=0$: The percolation cluster at p_c , the Sierpinski gasket and the T-fractal. Section III B is devoted to structures with a finite T_c , namely the

percolation cluster above p_c , the Sierpinski carpet and tobrene lattice. In Sec. IV we discuss the value of the exponent a_χ in all the cases considered, and the form of the fluctuation-dissipation plots. Section V contains a final discussion and the conclusions.

II. MODEL AND OBSERVABLES

The Ising model is defined by the Hamiltonian,

$$H[\sigma] = -J \sum_{\langle ij \rangle} \sigma_i \sigma_j, \quad (5)$$

where $\sigma_i = \pm 1$ is a unitary spin and $\langle ij \rangle$ are nearest neighbors on a graph.

The dynamics is introduced by randomly choosing a single spin and updating it with Metropolis transition rate

$$w([\sigma] \rightarrow [\sigma']) = \frac{1}{2} \min[1, \exp(-\Delta E/T)]. \quad (6)$$

Here $[\sigma]$ and $[\sigma']$ are the spin configurations before and after the move, and

$$\Delta E = H[\sigma'] - H[\sigma]. \quad (7)$$

We consider a system of N spins initially prepared in a high temperature uncorrelated state and then quenched, at time $t=0$, to a low final temperature T_f .

As already discussed, the dynamics of the spins in the bulk of domains provide the equilibrium contribution while what is left over accounts for the aging behavior. Since equilibrium dynamics is well understood, the stationary parts in Eqs. (1) and (2) are generally well known. In particular, at $T_f=0$ equilibrium dynamics is frozen and there are no stationary contributions. On the other hand, much interest is focused on the aging terms. These can be isolated by subtracting the stationary parts computed in equilibrium, from the whole quantity measured in the phase-ordering stage. This first method, however, is computationally very demanding. Therefore it is much more efficient to resort to a second, different method. This amounts to study a modified system where T_f in the transition rate (6) is set equal to zero if the spin to be updated belongs to the bulk, namely if it is aligned with all its neighbors. The bulk degrees of freedom, which alone contribute to the stationary parts, feel $T_f=0$; recalling that the equilibrium dynamics is frozen at $T_f=0$, and that, therefore, the stationary parts of the observables are zero, by computing quantities with this modified dynamics one isolates the aging terms. In doing so one has the evident advantage of simulating a single system and, moreover, to update only the spins on the interfaces, whose number in the late stage is a small fraction of the total degrees of freedom. Clearly this technique is meaningful if the properties of the aging terms are not affected by this modified dynamics with no bulk flips (NBF), as expected on the basis of the general idea that stationary and aging degrees of freedom are statistically independent. In order to prove this quantitatively, one can measure the aging part of an observable with the NBF technique and compare it with the same quantity obtained with the first method. This was done on regular lattices in Ref. [9], proving that the aging parts obtained with the two

methods are the same in the late stage. This allows one to use the modified dynamics to compute aging properties. All the results presented in the following are obtained with this method. Let us also mention that the NBF is a particular case of a more general Ising model with a local-field dependent temperature introduced in Ref. [10]. It can be shown [10] that letting $T_f=0$ in the bulk raises the critical temperature. This is expected since fluctuations in the bulk are suppressed. As a consequence, with NBF one can have phase ordering also for values of the temperature corresponding, with the standard dynamics, to a disordered phase. As we will discuss below, this fact may represent a formidable advantage on inhomogeneous graphs.

Let us discuss the case of graphs where a phase transition occurs at a finite critical temperature T_c . We denote these as systems of class I. For these structures we can consider quenches to finite temperatures $T_f < T_c$. The characteristic size $L(t)$ then grows until it becomes comparable with the system size and the new equilibrium state at T_f is globally attained. We always consider sufficiently large systems to prevent equilibration on the simulated time scales. The dynamics in this regime is equivalent to that of an infinite system, for which the final equilibrium state is never reached and $L(t)$ keeps growing indefinitely. By analogy with regular lattices, in the late stage one might expect the power law

$$L(t) \sim t^{1/z}, \quad (8)$$

although some caveats will be discussed in the following. On regular lattices the value $z=2$ is found quite generally. In the solution of the large- \mathcal{N} model on graphs [5] or in the framework of approximate theories [7] one finds $z=2d_f/d_s$, but such a relation is not expected for scalar systems.

Now we turn to systems of class II, namely those systems for which, with standard dynamics, $T_c=0$. For every finite T_f the system eventually equilibrate to a state with a finite coherence length $\xi(T_f)$, which diverges in the $T_f \rightarrow 0$ limit. If the temperature is sufficiently low, an interrupted phase ordering is observed until $L(t)$ becomes comparable with $\xi(T_f)$ and equilibration occurs. The phase-ordering phenomenon can be widened at will by decreasing T_f , and the scaling behavior with Eq. (8) can be studied. Quite generally, however, on inhomogeneous structures one cannot set $T_f=0$ directly, because this would freeze the dynamics due to pinning effects. For the same reason, also very low temperatures are not numerically accessible, since it takes an exponentially long time to surmount pinning barriers. From the numerical point of view, then, one must find a reasonable compromise between two contrasting issues. Namely, T_f must be sufficiently low in order to have a wide scaling regime preceding equilibration, but also sufficiently large to allow pinning barriers being overtaken. This may be in some cases impossible. Fortunately, the use of the NBF dynamics simplifies considerably the problem. As we have already pointed out, with NBF the critical temperature is raised. In the case of system where $T_c=0$ with standard dynamics, the effect of NBF is to move T_c from zero to some finite value. Then one has a whole low-temperature region where phase-ordering occurs asymptotically without being interrupted by equilibration, much alike in systems of class I. This allows to study the

scaling behavior also in this case. For all the reasons discussed above, in this paper we will always present results obtained with NBF dynamics.

Generally speaking, when scaling holds the characteristic length $L(t)$ can be estimated from the knowledge of the two-points equal time correlation function, obtained letting $t=s$ in Eq. (1),

$$G_{i,j}^{ag}(t) = \langle \vec{\sigma}_i(t) \cdot \vec{\sigma}_j(t) \rangle, \quad (9)$$

where $\langle \cdots \rangle$ means an ensemble average, namely taken over different initial conditions and thermal histories. In homogeneous systems according to Eq. (3) one has

$$G_{i,j}^{ag}(t) = G^{ag}(r, t) = g(x), \quad (10)$$

where $x=r/L(t)$. For scalar order parameter with sharp interfaces, a short distance behavior ($x \ll 1$) of the type $1-g(x) \sim x$ is found [1,11], namely a Porod's tail $\hat{g}(u) \sim u^{-(d+1)}$ in momentum space for large $u=kL(t)$. With Eq. (10) the characteristic length can then be evaluated, for instance, as the half-height of $G(r, t)$, namely from the condition

$$G^{ag}[r=L(t), t] = \frac{1}{2}G^{ag}(0, t). \quad (11)$$

On usual lattices the size of domains can be easily related to the density of interfaces $\rho(t)$. In fact, since domains are compact, the ratio between their surface and their volume is proportional to $L(t)^{-1}$ and one has $\rho(t) \sim L(t)^{-1}$. Since asymptotically $\rho(t)$ has a power-law behavior

$$\rho(t) \sim t^{-\theta}, \quad (12)$$

this implies

$$\theta = 1/z. \quad (13)$$

In homogeneous structures, then, $\rho(t)$ provides an indirect, alternative method for the determination of $L(t)$, and hence of z .

On generic graphs the notion of a distance is not as straightforward as on regular lattices and, considering the correlation function (9) one should, in principle, retain the full dependence of $G_{i,j}(t)$ on i and j . This would be a formidable task without probably providing much insight into the physics and, in particular, into the scaling behavior. On the other hand, once a notion of a distance is adopted, the behavior of $G(r, t)$, and in particular its scaling properties, may depend on the distance used. For these reasons we do not have a simple recipe for inferring scaling behaviors from equal time correlation functions. Then, in order to provide at least an evidence of the dynamical scaling symmetry for some of the structures considered in Sec. III, we will introduce a definition of distance along a *natural* direction (usually the border of the structure). With this definition, we will check the validity of Eq. (10) and we will compute $L(t)$ through Eq. (11). We stress, however, that the validity of this procedure is limited to the particular definition of distance used. Another, independent, approach to the analysis of the scaling behavior, which does not imply the notion of a distance, is provided by the two time quantities.

The two time quantities that will be considered in this paper are the (spatially averaged) autocorrelation function

$$C(t, s) = \frac{1}{N} \sum_{i=1}^N \langle \sigma_i(t) \cdot \sigma_i(s) \rangle \quad (14)$$

and the integrated (auto)response function

$$\chi(t, s) = \int_s^t dt' R(t, t'). \quad (15)$$

The quantity

$$R(t, t') = \frac{1}{N} \sum_{i=1}^N \left. \frac{\partial \langle \sigma_i(t) \rangle}{\partial h_i(t')} \right|_{h=0}, \quad (16)$$

is the (spatially averaged) linear response function associated to the perturbation caused by an impulsive magnetic field h_i switched on at time $t' < t$.

On regular lattices, scalings (3) and (4) and power-law growth of $L(t)$ imply

$$C^{ag}(t, s) = h(y) \quad (17)$$

and

$$\chi^{ag}(t, s) = s^{-a} \chi f(y), \quad (18)$$

where $y=t/s$ and $h(y)=\mathcal{C}(0, y)$, $f(y)=\tilde{\chi}(0, y)$, and the large- y behaviors

$$h(y) \sim y^{-\lambda}, \quad (19)$$

$$f(y) \sim y^{-a_\chi}. \quad (20)$$

Equations (17) and (18) may be used to check if dynamical scaling is obeyed, avoiding the problems related to the definition of a distance affecting $G^{ag}(r, t)$. Let us mention, by the way, that in our simulations the same conclusions about the existence of the scaling symmetry are provided by $G^{ag}(r, t)$ (with a definition of distance along a *natural* direction, as discussed above) and by $C^{ag}(t, s)$.

In order to compute $\chi(t, s)$ we enforce the out of equilibrium generalization of the fluctuation dissipation theorem derived in Refs. [12–14], which relates the response function to particular correlation functions of the unperturbed system

$$T\chi(t, s) = \frac{1}{2} \left(C(t, t) - C(t, s) - \int_s^t \langle \sigma_i(t) B_i(t') \rangle dt' \right), \quad (21)$$

where

$$B_i[\sigma] = - \sum_{\sigma'} (\sigma_i - \sigma'_i) w([\sigma] \rightarrow [\sigma']). \quad (22)$$

In this equation $[\sigma]$ and $[\sigma']$ are two configurations differing only by the spin on site i , taking the values σ_i and σ'_i , respectively. This relation allows to compute the integrated response function by measuring correlation functions on the unperturbed system, avoiding the complications of the traditional methods where a perturbation is applied, and improving significantly the quality of the results [14].

Finally, let us notice that the relation (13) does not hold on generic networks, as we will show explicitly in our simu-

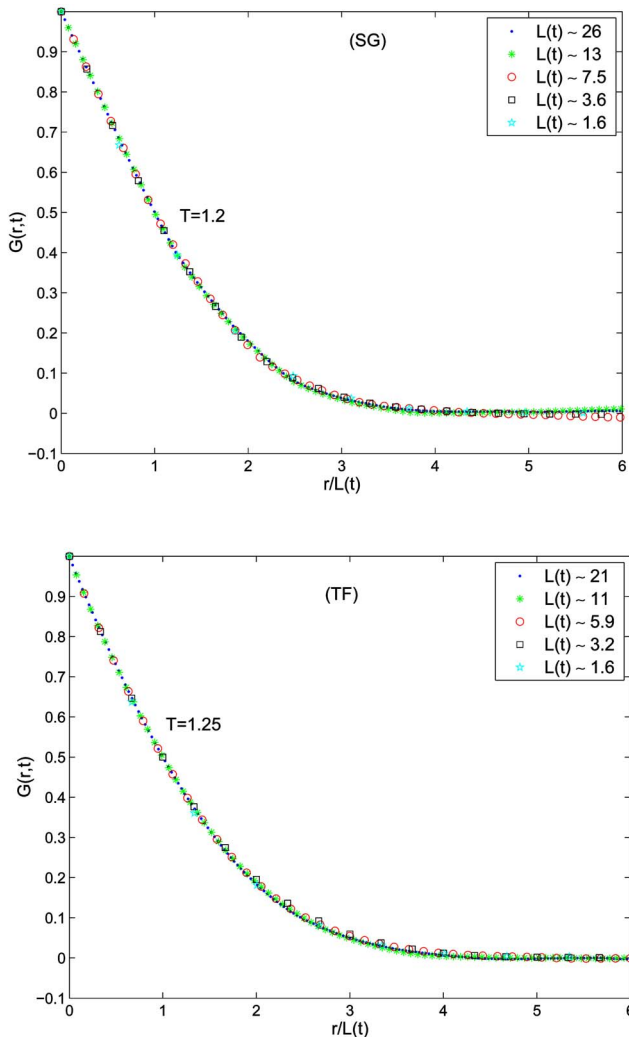


FIG. 2. (Color online) $G_{ag}^{ag}(r,t)$ is plotted against $x=r/L(t)$ for the (TF) and the (SG), the time t ranges from 10 steps for the shortest $L(t)$ to 400 000 for the longest lengths.

lations. Actually, as will be discussed in Sec. III A, the number of spins on the surface of a domain of size $L(t)$ may depend dramatically on (among other parameters) the quench temperature. Therefore, in general, there is not a unique relation between $\rho(t)$ and $L(t)$ and they provide independent informations.

III. NUMERICAL SIMULATIONS

In the following we will present the numerical results. We set $J=1$. Statistical errors are comparable to the thickness of the symbols. We recall that NBF dynamics is always used, and therefore we measure directly the aging part of every observable considered.

A. Graphs with $T_c=0$

Let start with systems of class II, first. The structures considered in the simulations will be the Sierpinski gasket (SG), the T-fractal (TF), and the percolation cluster (PC),

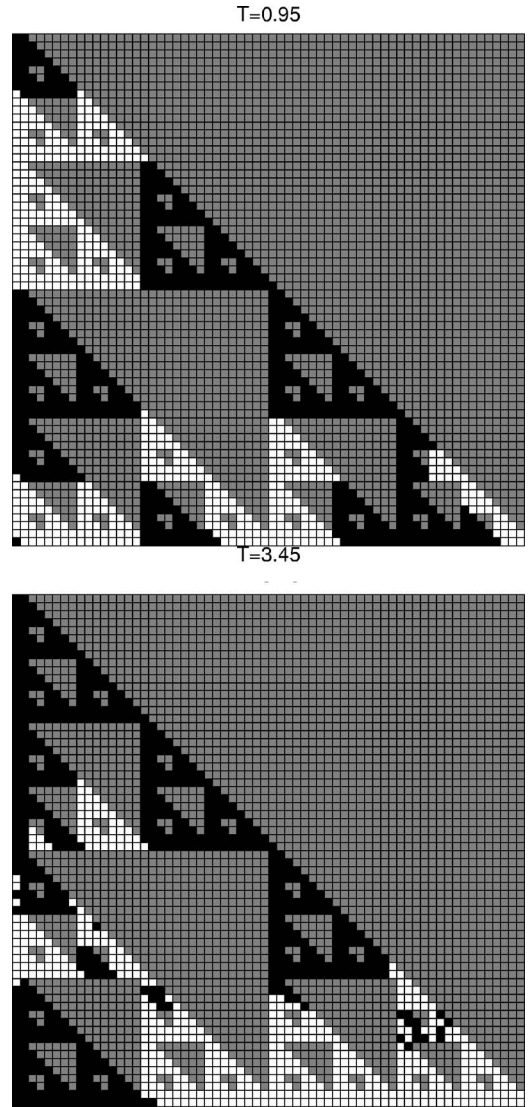


FIG. 3. (SG) Two spin configurations after $t=1000$ steps for the temperatures $T_f=0.95$ and $T_f=3.45$.

namely a diluted square lattice, at the the percolation threshold (see Fig. 1). All these structures are finitely ramified, i.e., each arbitrary large part can be disconnected by cutting a finite number of links and, in particular, the SG and the TF are exactly decimable [8]. The SG and the TF are deterministic fractals, with $d_F=\ln 3/\ln 2$ and $d_F=\ln 3/\ln 2$, and $d_s=2\ln 3/\ln 5$ and $d_s=2\ln 3/\ln 6$, respectively. The PC is a random fractal, so that in this case the results presented are averages over different topological realizations. The d_F and d_s of the PC have been estimated numerically and with renormalization procedures and their values are $d_F=1.82$ and $d_s=4/3$. The number N of spins in this structures is 265 722 and 531 442 for the SG, and TS, respectively. The PC has been obtained by means of site percolation on a square lattice of size 1200 at the critical dilution $p_c=0.407$. The results presented are thermal and topological averages over 100 realizations.

As we already pointed out in the preceding previous section, there is not a natural definition of distance on graphs. For the SG, we have chosen to compute the equal time cor-

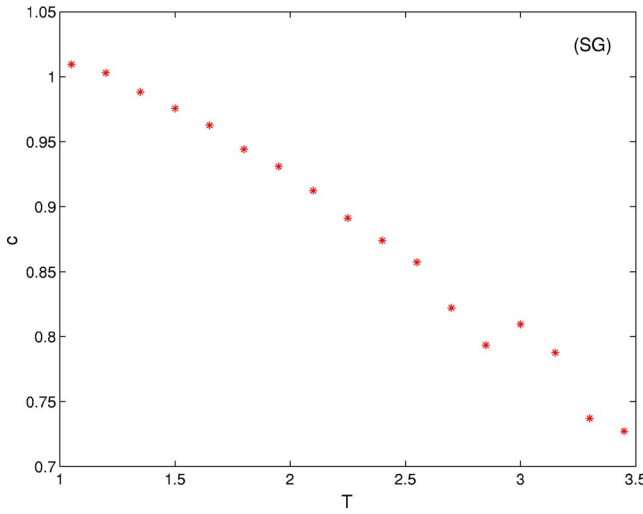


FIG. 4. (Color online) (SG) The exponent c characterizing the behavior of $g(x)$ for $x=0$.

relation function (9) by restricting i and j along the borders of the structure. We do this because along these lines all sites are occupied by spins and therefore the distance between them can be naturally defined as on regular lattices. For the same reason, in the TF we have computed $G^{ag}(r,t)=G_{ij}^{ag}(t)$ for points i and j along the baseline of the structure.

In Fig. 2, $G^{ag}(r,t)$ is plotted against $x=r/L(t)$ for the SG and the TF. One finds a very good data collapse, as expected on the basis of Eq. (10). This indicates that, with respect to particular directions used for calculating $G^{ag}(r,t)$, dynamical scaling is obeyed on these structures. Notice also the presence of the Porod's tail, for small x , implying that interfaces are sharp objects at the relatively low temperatures considered in Fig. 2. However, when the temperature is raised, the interfaces broaden on the fractal substrate, as shown in Fig. 3. Here one expects a deviation from the Porod linear behavior. This can be clearly seen in Fig. 4. Here we plot the exponent c which regulates the small x decay of $g(x)$, namely $1-g(x) \sim x^c$, as a function of T_f .

The characteristic size $L(t)$, obtained as in Eq. (11), is shown in Fig. 5. This length grows roughly as a power law, but with a superimposed oscillation which is more pronounced at low temperatures. These log-periodic oscillations are very reminiscent of what one observes in the related problem of Brownian motion on this structure [15] and in short time dynamics simulations on the SC [16], indeed they can be linked to the discrete symmetry invariance of fractals [17]. In our case they originate as an effect of pinning forces acting on the growth of clusters at different discrete scales. In fact, as shown schematically in Fig. 6 for the SG, if two triangles happen to be ordered differently, in order to start reversing one of the two to achieve a global ordering, one must flip one of the interfacial spins, for example, the one marked with an arrow. This move requires an activation energy $\Delta E=4J$ and can then be accomplished on a time $\tau \approx \exp(4J/T_f)$. The dynamics then proceeds without activated processes until all the triangle is reversed but, then, a new activated step is required and so on. During the time τ the dynamics on the triangle in consideration is frozen. Since all

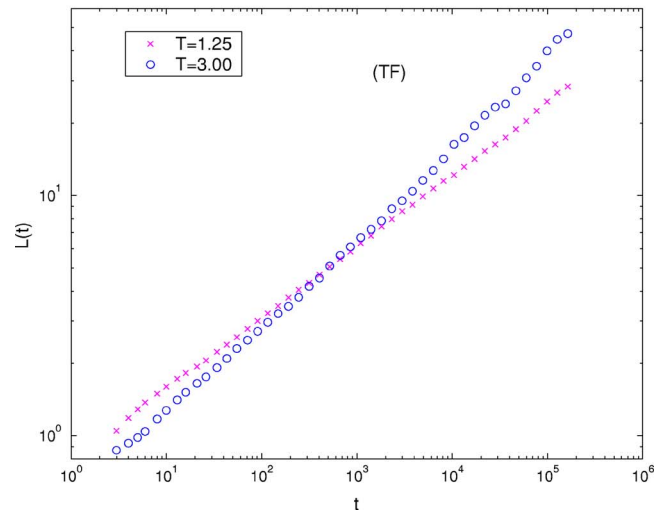
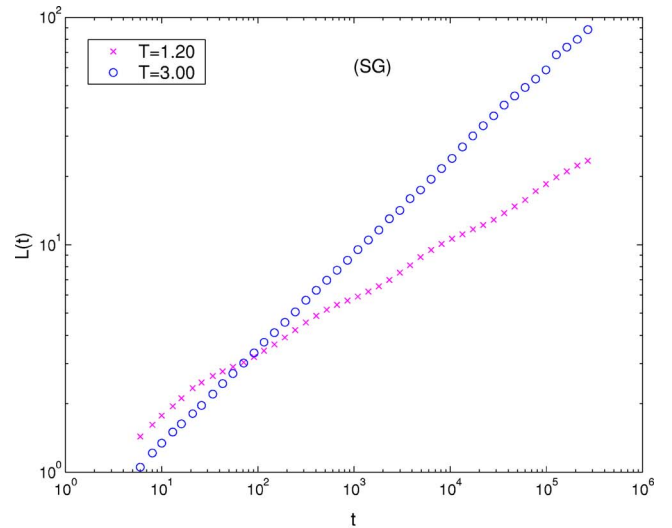


FIG. 5. (Color online) The characteristic length $L(t)$ is plotted against t , for two different temperatures $T_f=1.2$ and $T_f=3.0$ for the (SG) and $T_f=1.25$ and $T_f=3.0$ for the (TF).

the triangles have the same qualitative behavior, with some fluctuations, the overall behavior of $L(t)$ shows a periodic oscillation due to the recurring slow down caused by activated processes. An analogous phenomenon occurs in the TF. Clearly, since τ decreases at larger temperatures, this phenomenon is less evident, although still present even at relatively high temperatures, as shown in Fig. 5.

The curves of Fig. 5 can be quite convincingly fitted by a power law with periodic oscillations superimposed. The exponent z of the power law, however, should be thought of as an effective exponent resulting from the balance between nonactivated processes obeying a growth law (8) with a certain value of z , and the activated processes whose net effect is an overall slowing down. Since the relative importance of these two processes is regulated by T_f , z turns out to be temperature dependent, as shown in Fig. 7. On the basis of the previous discussion, one would expect to have a faster growth, namely a larger $1/z$, for higher T_f . This is indeed observed in Fig. 7 in a broad range. For very large temperatures $1/z$ seems to saturate. This is perhaps due to the neigh-

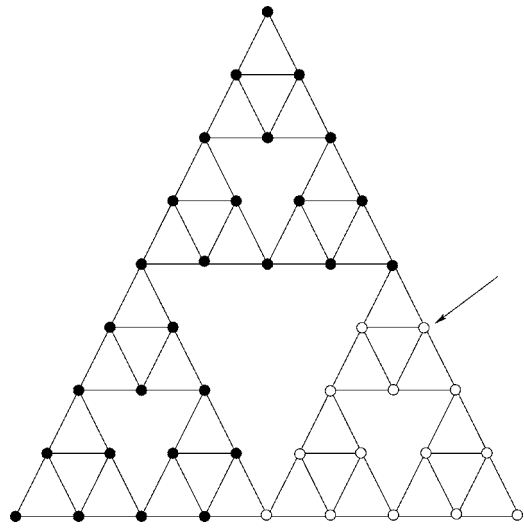


FIG. 6. Schematic representation of a part of the structure, showing the necessity of activated processes.

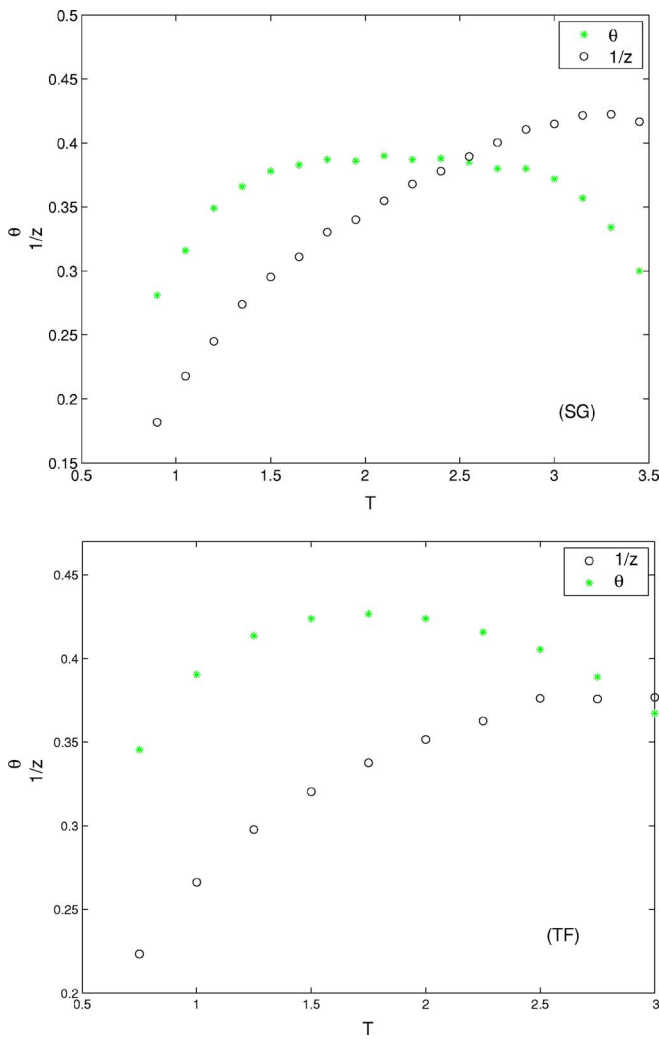


FIG. 7. (Color online) The dependence on temperature of the exponents $1/z$ and θ for the (SG) and the (TF).

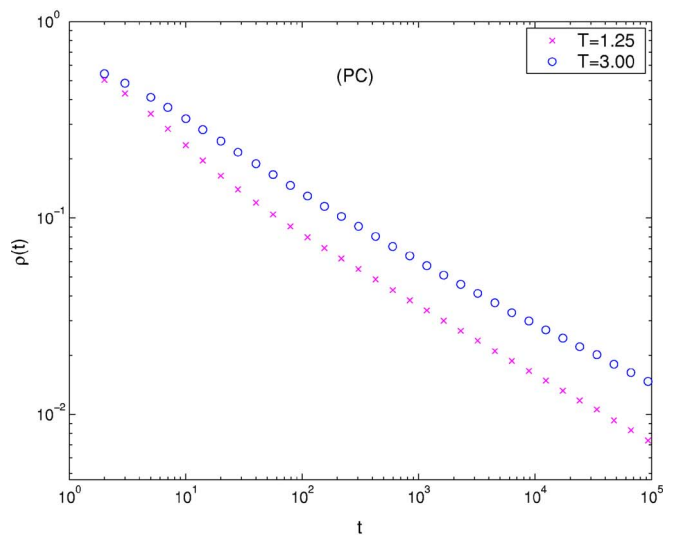
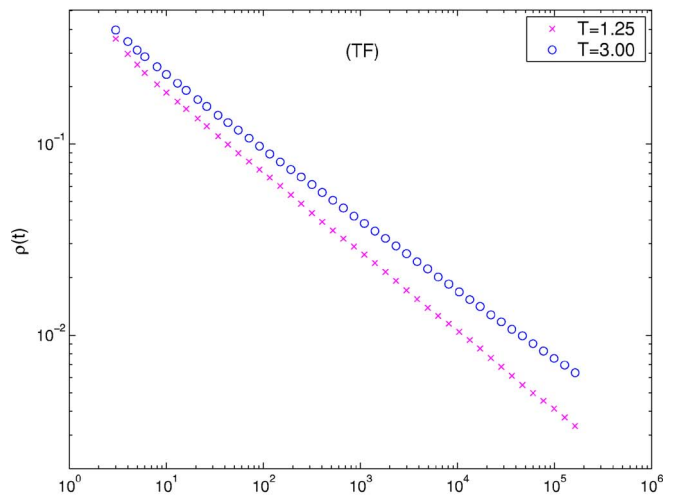
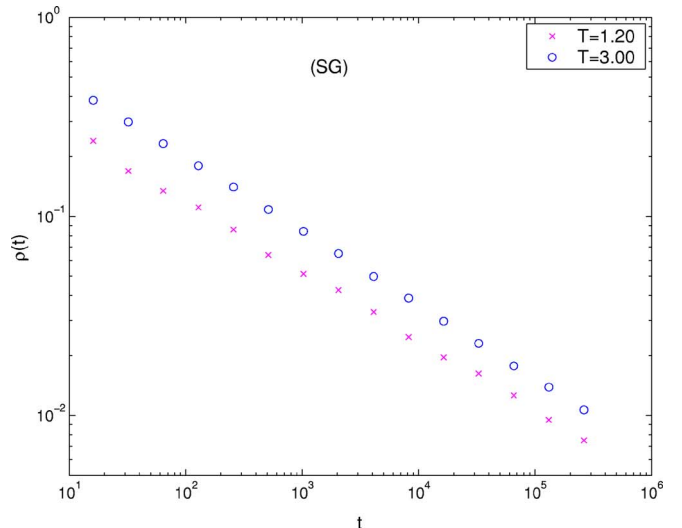


FIG. 8. (Color online) The density of interfaces $\rho(t)$ is plotted against t , at the temperatures $T_f=1.2$ and $T_f=3$ for the (SG), at $T_f=1.25$ and $T_f=3$ for the (TF) and (PC).

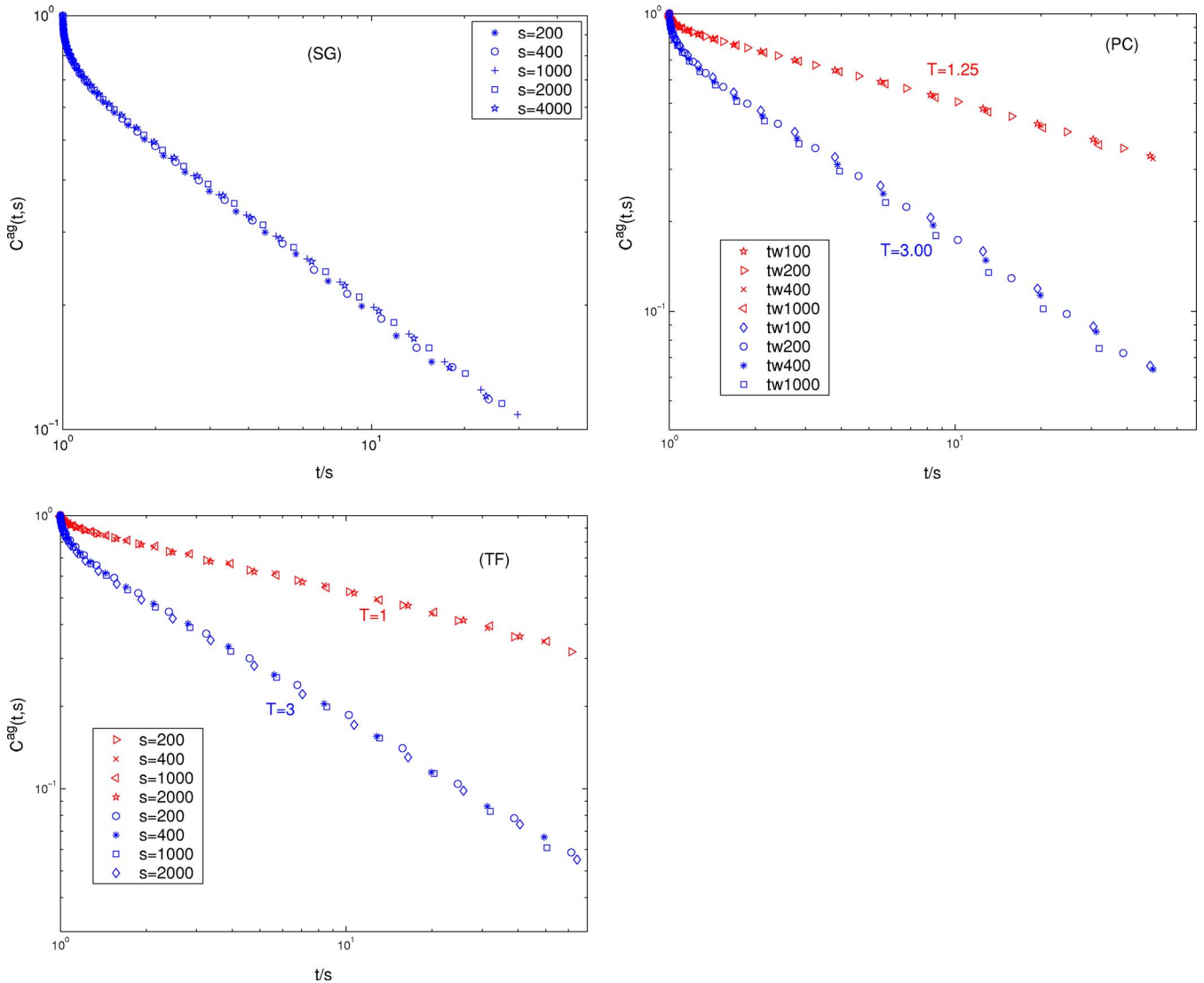


FIG. 9. (Color online) (SG) $C_{ag}(t,s)$ is plotted against $y=t/s$, at $T_f=3$ for the (SG), at $T_f=3$ and $T_f=1$ for the (TF) and at $T_f=3$ and $T_f=1.25$ for the (PC).

borhood of the critical temperature (that with NBF turns out to be $T_c \simeq 3.6$ and $T_c \simeq 2$ for the SG and the TF, respectively), slowing down the dynamics much in the same way as it happens on regular lattices.

A pattern similar to that of $L(t)$ is observed for $\rho(t)$. This quantity, defined as the density of spin which are not fully aligned with their neighbors, is shown in Fig. 8 for the SG, TF and PC. Also in this case one observes oscillations on top of the power-law behavior (12). The value of θ also depends on temperature, as shown in Fig. 7. Differently from $1/z$, however, the behavior is strongly nonmonotonous, with a broad maximum at intermediate temperatures. As already observed, the exponent θ and $1/z$ are not trivially related, as on homogeneous structures. In the limit of low temperatures one finds an exponent θ consistent with $\theta = -d_f/z$, which can be understood on the basis of the following argument. Let us consider again, for simplicity, the SG of Fig. 6. When the temperature is very low interfaces are very likely located in the pinning positions, as can be seen in Fig. 3. A domain, therefore, is a triangle of size $L(t)$, with a volume $V \propto L(t)^{d_f}$,

and a number of surface spins $n_s = 3$. The density of interfacial spins is, therefore $\rho(t) \sim L(t)^{-d_f}$. One then has

$$\theta = -\frac{d_f}{z}, \quad (23)$$

instead of Eq. (13), holding on regular lattices. Let us remark again, however, that, although this relation is consistent with our data in the limit of small T_f , it is not of general validity. Actually, as already evident from Fig. 3 and from the non-linear behavior of $g(x)$ at small x , for larger temperatures, interfaces are no longer located on the pinning centers.

Let us consider now the behavior of two time quantities. The autocorrelation function for the SG, TF, and PC are plotted in Fig. 9 against $y=t/s$. According to Eq. (17), one should observe data collapse of the curves with different s . This is indeed observed, further supporting the evidence of dynamical scaling. One also finds the large- y -power law behavior (19) with an exponent λ strongly dependent on temperature. Let us turn to consider the response function. Ac-

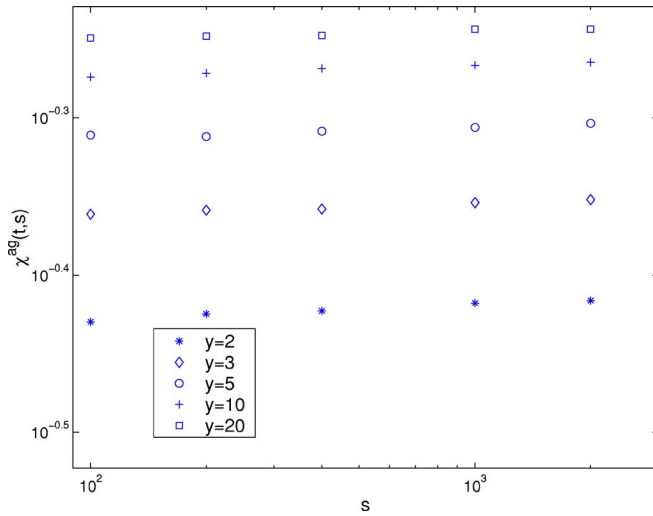


FIG. 10. (Color online) (TF) $\chi^{ag}(t,s)$ is plotted against s for fixed values of $y=t/s$, for $T_f=3$.

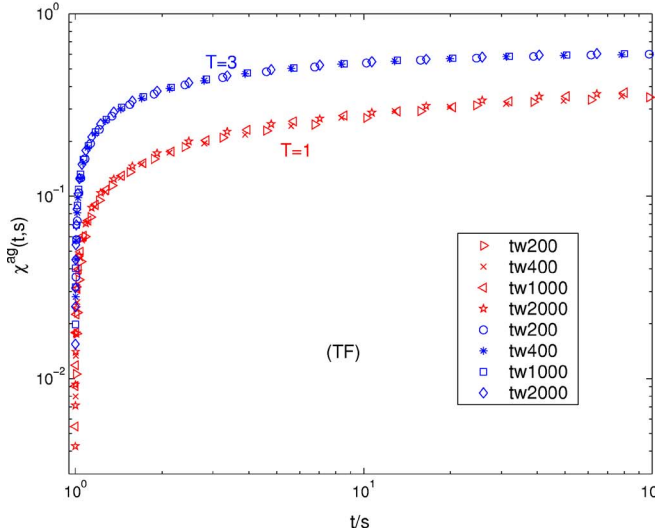
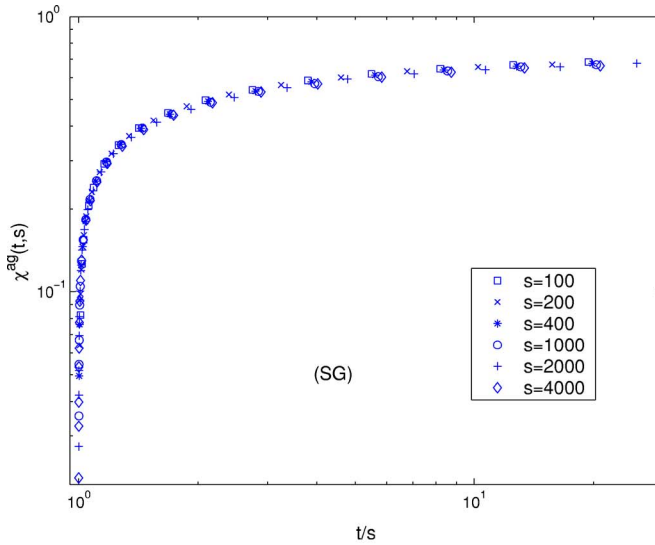
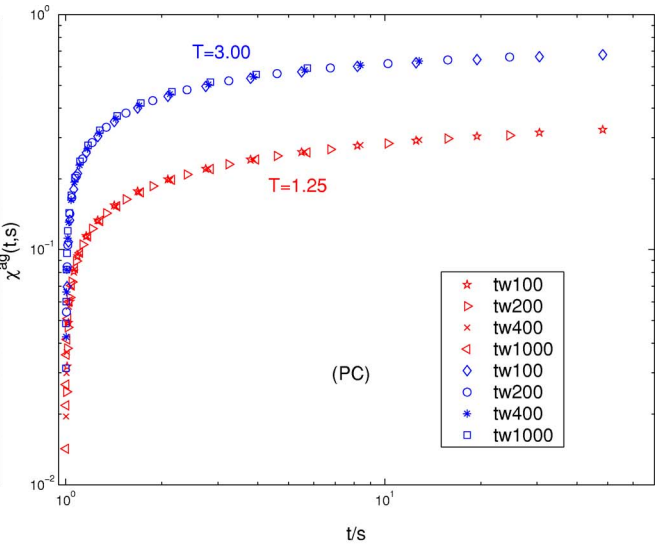


FIG. 11. (Color online) (SG) $\chi^{ag}(t,s)$ is plotted against $y=t/s$ for different values of s , for $T_f=3$ (SG), $T_f=3$, and $T_f=1$ (TF) and for $T_f=3$ and $T_f=1.25$ (PC).

cording to Eq. (18) the exponent a_χ can be obtained as the slope of a double logarithmic plot of $\chi^{ag}(t,s)$ against s , with y held fixed. Such determination should be independent of y , within errors. We show this plot in Fig. 10 for the TF. We obtain $a_\chi=0.01\pm 0.02$ which is consistent with $a_\chi=0$, similarly to that found in homogeneous systems with $T_c=0$ [19–21]. Analogous values are found for all the structures with $T_c=0$. Then, by plotting $\chi^{ag}(t,s)$ against y one should find data collapse, how it is indeed shown in Fig. 11 for the SG, TF, and PC at different temperatures. In conclusion, the autocorrelation and response function obey the expected scaling forms (17) and (18).

B. Graphs with $T_c > 0$

In this section we will consider systems of class I. In particular we will study the phase-ordering kinetics on the diluted square lattice (DS) above the percolation threshold, the *toblerone* lattice (TL) obtained by replicating the Sierpin-



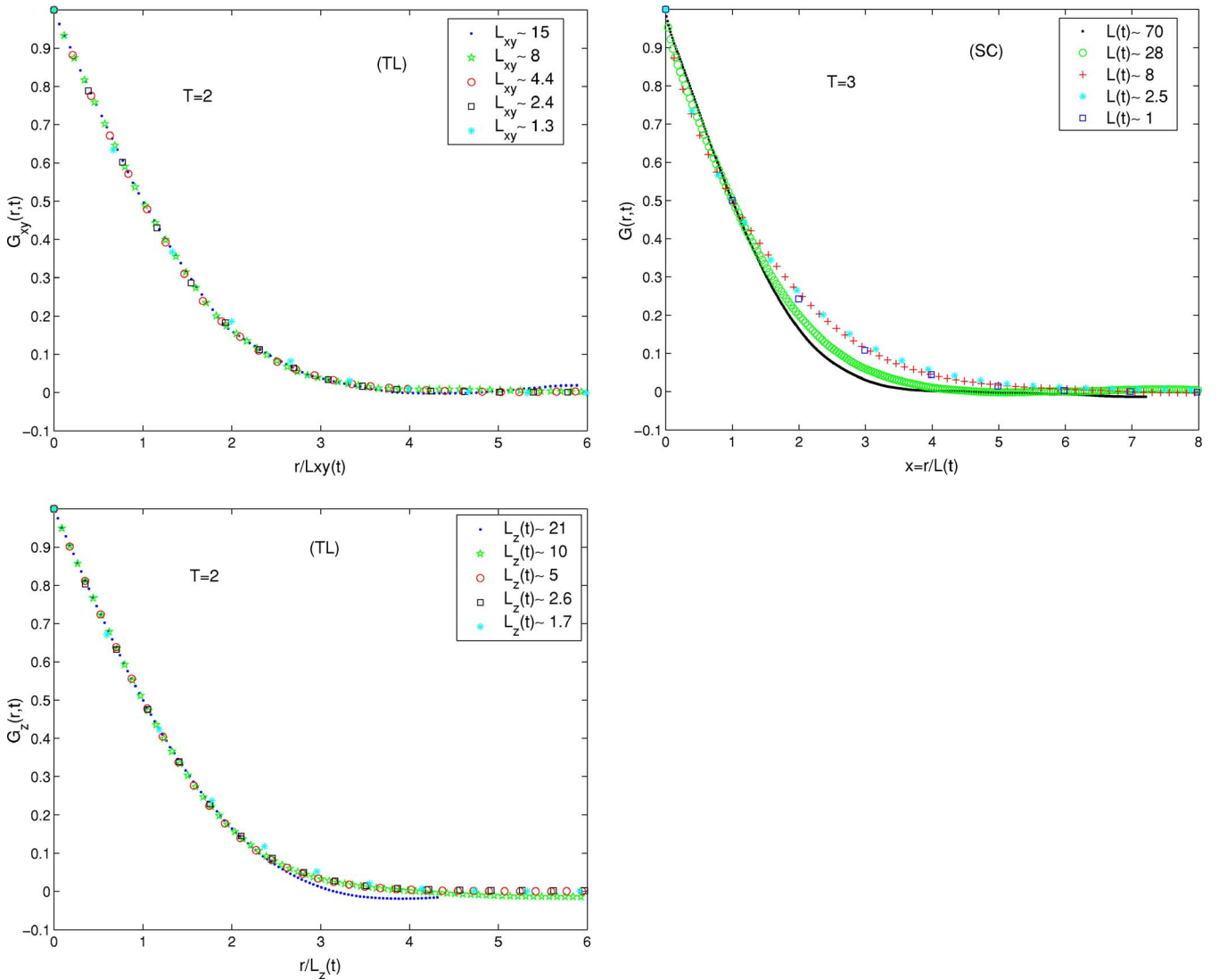


FIG. 12. (Color online) For the (TL) we plotted $G_{xy}^{ag}(r,t)$ and $G_z^{ag}(r,t)$ against $x=r/L(t)$ for the (SC) we plotted $G^{ag}(r,t)$.

ski gasket along a third spatial direction z , and the Sierpinski carpet (SC). These structures are represented in Fig. 1 and they all have infinite ramification. The SC is a deterministic fractal with $d_f = \ln 8 / \ln 3$ and d_s estimated to be 1.81. The dynamics of the SC has been previously studied numerically in quenches at T_c in Refs. [16,18] and below T_c in the framework of the time-dependent Ginzburg-Landau equation in Ref. [7]. The TL is a physical graph, obtained by the direct product of a SC with a linear chain, and therefore it presents anisotropic behavior along different directions. Its d_f and d_s are the sum of the respective dimensions of the SC and of the linear chain $d=1$. The DS is a random structure with the same large scale topology of a two-dimensional regular lattice.

For the SC, we have computed the equal time correlation function (9) along the borders of the structure, analogously to what was done for the SG. The TL is an anisotropic structure, since it is translational invariant along the z direction alone. Therefore we have computed the equal time correlation function on the planes with a constant z , and in the z direction separately. These are denoted as $G_{xy}^{ag}(r,t)$ and

$G_z^{ag}(r,t)$, respectively. The former is computed along the borders of the structure, as for the SG. In Fig. 12 $G^{ag}(r,t)$ is plotted against $x=r/L(t)$ for the TL and the SC. One finds a good data collapse for the TL, as expected on the basis of Eq. (10). The scaling is not observed for the SC in the range of times accessed in our simulations. Notice also in these cases, the presence of the Porod's tail, for small x , implying that interfaces are sharp objects at low temperature. As in the case of the SG, when the temperature is raised the interfaces broaden and the Porod behavior does not hold.

The characteristic size $L(t)$, obtained as in Eq. (11), is shown in Fig. 13. For the TL there are two different lengths $L_{xy}(t)$ and $L_z(t)$ obtained from $G_{xy}^{ag}(r,t)$ and $G_z^{ag}(r,t)$, respectively. Also in this case the presence of log periodic oscillations on top of an average power-law growth is observed. Similarly to the case discussed in Sec. III A, this phenomenon is due to pinning forces. As shown schematically in Fig. 14, in fact, the length of an interface is decreased if it crosses the holes of the structures, as in the configurations (A) and (C), which are local energy minima. In order to evolve from (A) to (C), the interface must move to configu-

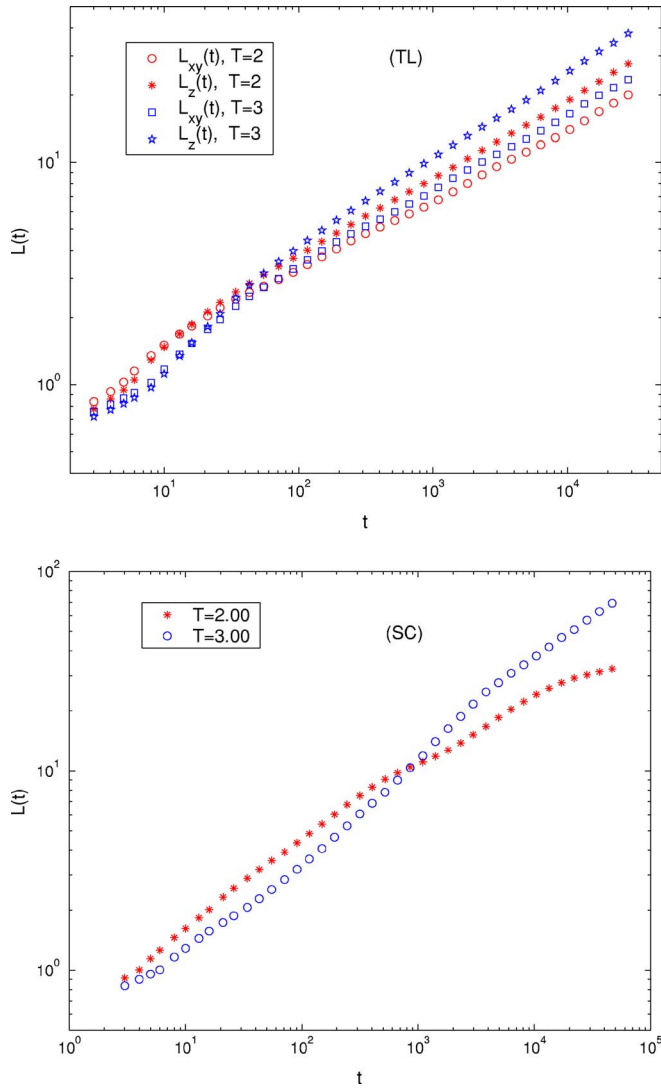


FIG. 13. (Color online) For the TL the characteristic lengths $L_{xy}(t)$ and $L_z(t)$ are plotted at the temperatures $T_f=2$ and $T_f=3$. For the (SC) $L(t)$ is plotted against t , at $T_f=2$ and $T_f=3$.

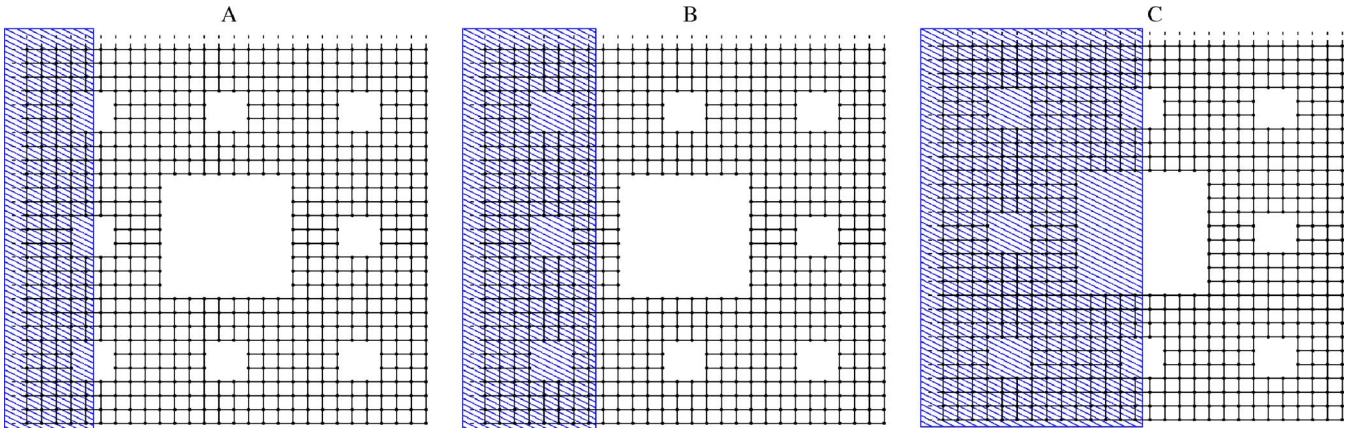


FIG. 14. (Color online) Schematic representation of a cluster (shaded region) on a SC evolving from configuration (A)–(C).

ration (B), which requires activated processes. Therefore in this case the oscillations can be related to the energy pinning acting not on a single site, as for the SG, but on an extended boundary. For the SC the exponent z is $z=0.33$ and $z=0.45$ at $T_f=2$ and $T_f=3$. The behavior of $\rho(t)$ is similar to that found for the structures with $T_c=0$, discussed in Sec. III A. This quantity, is shown in Fig. 15 for the DS, TL, and SC. For the SC, $\theta=0.38$ and $\theta=0.43$ at $T_f=2$ and $T_f=3$. Therefore also on these structures both θ and z depend on the temperature.

Let us consider now the behavior of two time quantities. The autocorrelation function for the DS, TL, and SC are plotted in Fig. 16 against $y=t/s$.

For the TL one has a good data collapse for the larger values of s , according to Eq. (17). The situation is different for the DS and SC. In these cases, there is no data collapse in the figure. Therefore, from the analysis of both $G^{ag}(r,t)$ and $C^{ag}(t,s)$ one can conclude that dynamical scaling is not observed in the range of time accessed in our simulation on the infinitely ramified fractals considered in this paper, while it is obeyed on the TL.

Let us turn to consider the response function. From $\chi^{ag}(t,s)$ we extract a_χ as the slope of a double logarithmic plot of $\chi^{ag}(t,s)$ against s , with y held fixed, as described regarding Fig. 10. We obtain $a_\chi=0.21$, $a_\chi=0.25$, and $a_\chi=0.18$ for the DS, the TL and the SC, respectively. Plotting $s^{a_\chi}\chi^{ag}(t,s)$ against y we find a good data collapse, independently from the temperature, as shown in Fig. 17, indicating that Eq. (18) is obeyed. Also the large- y behavior (20) is obeyed. Let us stress that, interestingly, $\chi^{ag}(t,s)$ obeys the scaling forms (18) and (20), even when the analysis of both $G^{ag}(r,t)$ and $C^{ag}(t,s)$ implies that scaling is not obeyed, as for the DS and SC.

IV. THE RESPONSE FUNCTION EXPONENT AND THE FLUCTUATION DISSIPATION PLOT

In the preceding section, we have checked the validity of the scaling form (18) in the fractal structures considered, and we have determined the value of the exponent a_χ . As already emphasized, while all the other quantities turn out to be very

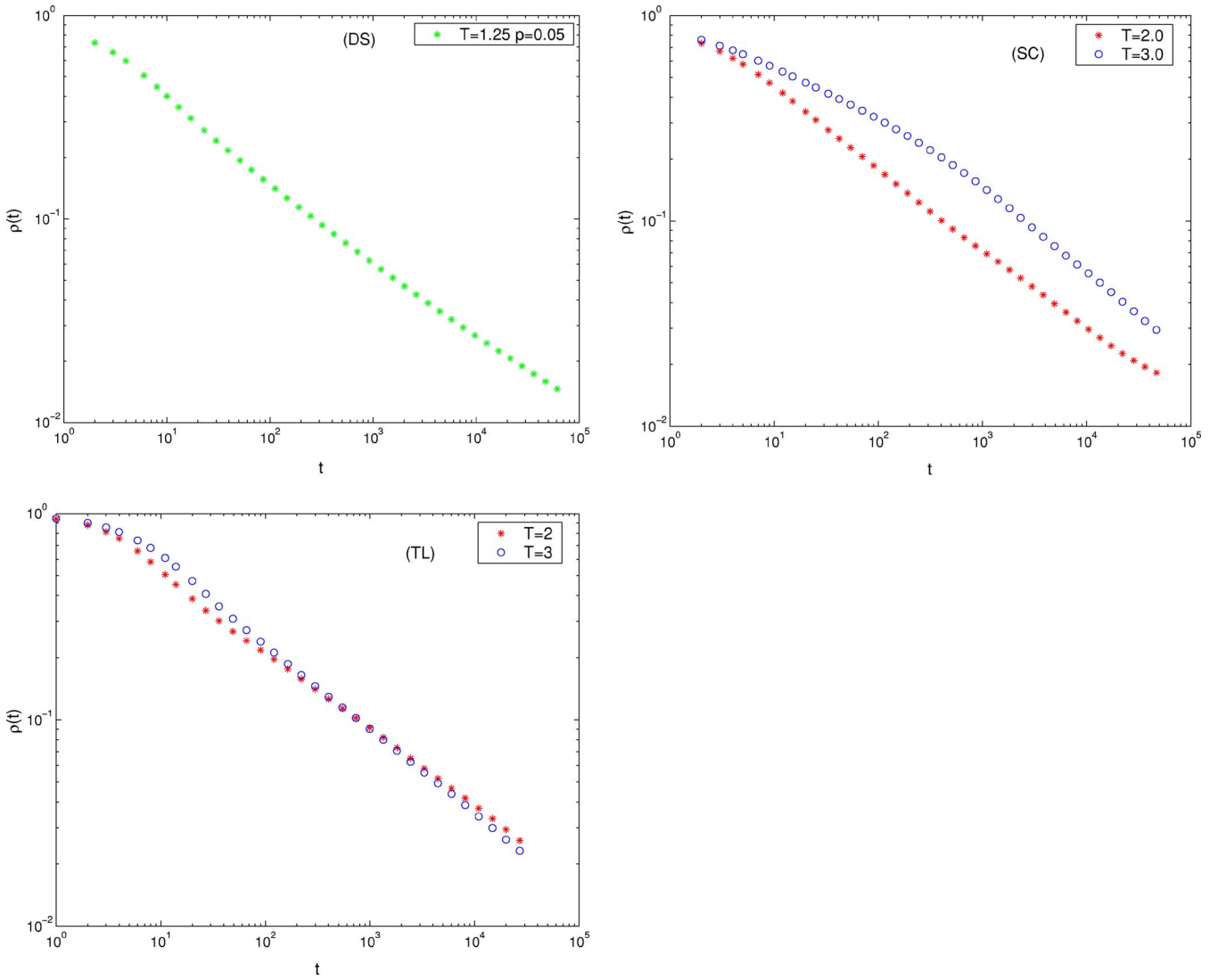


FIG. 15. (Color online) (DS) The density of interfaces $\rho(t)$ is plotted against t , at the temperature $T_f=1.25$ for the (DS), at $T_f=2$ and $T_f=3$ for the (TL) and for the (SC).

sensitive to the final temperature of the quench, this exponent assumes a well-defined value in all the low temperature region. On regular lattices, analytical calculations in the vector $O(\mathcal{N})$ model in large- \mathcal{N} limit [22] find the following dependence on dimensionality:

$$a_\chi = \begin{cases} \theta \frac{d - d_L}{d_U - d_L} & \text{for } d < d_U, \\ \theta & \text{with ln corrections for } d = d_U, \\ \theta & \text{for } d > d_U, \end{cases} \quad (24)$$

where d_L is the lower critical dimension of static critical phenomena and $d_U=4$. Numerical simulations [21,23,24] of discrete and $O(\mathcal{N})$ vectorial systems, with conserved and nonconserved order parameter, are consistent with Eq. (24), and $d_U=3$ or $d_U=4$ for scalar or vectorial models, respectively. This shows that the nonequilibrium exponent, a_χ , is related in a nontrivial way to the topology of the underlying

lattice, through d . Interestingly, this relation implies $a_\chi > 0$ when the system is above d_L , i.e., when a phase transition at finite temperature T_c is present, $a_\chi=0$ at d_L and $a_\chi < 0$ below d_L . This result for regular lattices suggests that the nonequilibrium dynamics of statistical models, and in particular the response function exponent, could be related to important topological properties also in the case of generic graphs. This hypothesis can be checked in some detail in systems with a continuous symmetry, because in this case it is well known that a large scale parameter, the “spectral dimension” d_s , encodes the relevant topological features, uniquely determines the existence of phase transitions [25] and controls the critical behavior [26]. In other words on generic networks d_s plays the same role played by the Euclidean dimension d on regular lattices. In particular, vectorial models on graphs exhibit a phase transition at finite temperature only if $d_s > d_L = 2$. Solving an $O(\mathcal{N})$ model in the large- \mathcal{N} limit [6] one can show that this property holds true also for the nonequilibrium exponent a_χ . In fact, one finds the same expression (24) as for regular lattices, with d_s replacing d . Then, again one has

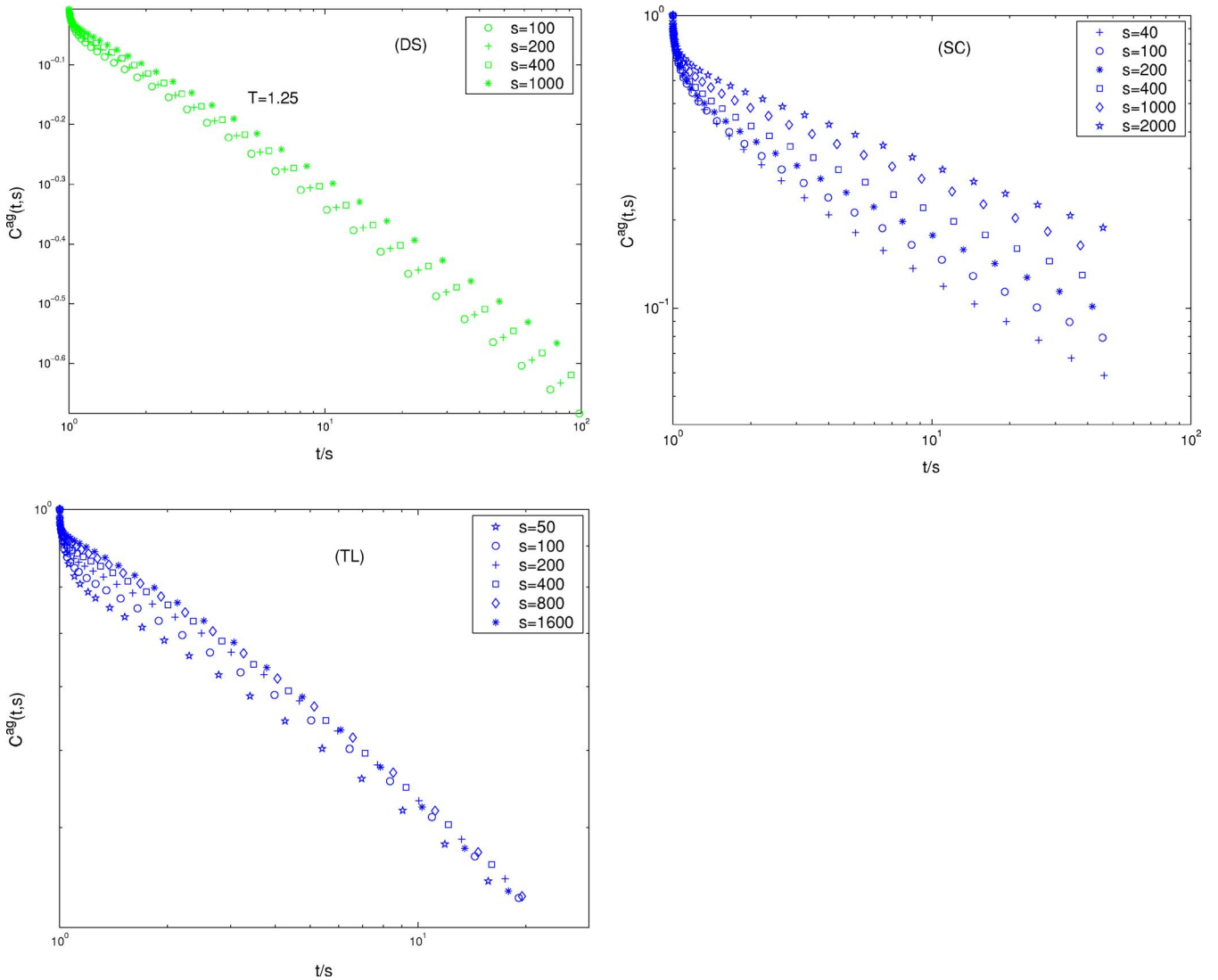


FIG. 16. (Color online) (DS) $C^{ag}(t,s)$ is plotted against $y=t/s$, at $T_f=1.25$ for the (DS) and at $T_f=3$ for the (TL) and (SC).

$a_\chi > 0$ when the system is above d_L , i.e., when a phase transition at finite temperature T_c is present, and $a_\chi \leq 0$ when $T_c=0$ [6]. The conclusion is that, for models with a continuous symmetry there is a well-defined relation between the nonequilibrium exponent a_χ and the topological features of the network which regulate the critical properties. In this case, this features are totally described by a single index, namely d_s . The next question is if a similar picture holds for scalar systems, where the counterpart of d_s is not known. Namely, if the nonequilibrium exponent a_χ is related to the critical properties, and in turn to topology, such that $a_\chi > 0$ or $a_\chi \leq 0$ holds for graphs with $T_c > 0$ or $T_c=0$, respectively. An argument [6] based on the topology of class II networks suggests that $a_\chi=0$ is expected for these systems. The values of a_χ reported in Sec. III show quite convincingly that the above conjecture is verified in all the cases considered in our simulations. One has $a_\chi \approx 0$ in all the structures of class II and $a_\chi > 0$ in those of class I. This result is particularly interesting for discrete symmetry models. In fact, while for $O(N)$ models the presence of phase transition can be inferred from d_s , there is not such a general criterion for discrete

models. Our data suggest that a_χ may be used to infer the presence of phase transition on a generic network. We recall again that this result directly links a_χ to some relevant topological features of graphs. For this reason, although a_χ is a nonequilibrium dynamical exponent, it is totally independent of all the nonuniversal details of the dynamics we have described in Sec. III. We have already observed, in fact, that, differently from all the other dynamical exponent, its value is robust and temperature independent.

Finally, we mention that the value $a_\chi=0$ found in the structures of class II is associated to an anomalous fluctuation-dissipation plot [23]. Reparametrizing in $\chi(t,s)$ the time t in terms of $C(t,s)$, according to the theorem by Franz, Mezard, Parisi, and Peliti [27], under broad hypotheses the relation

$$-T_f \lim_{s \rightarrow \infty} \left. \frac{d^2 \chi(C,s)}{dC^2} \right|_{C=q} = P_{eq}(q) \quad (25)$$

exists between the nonequilibrium two time functions χ , C and the equilibrium probability distribution $P_{eq}(q)$ of the

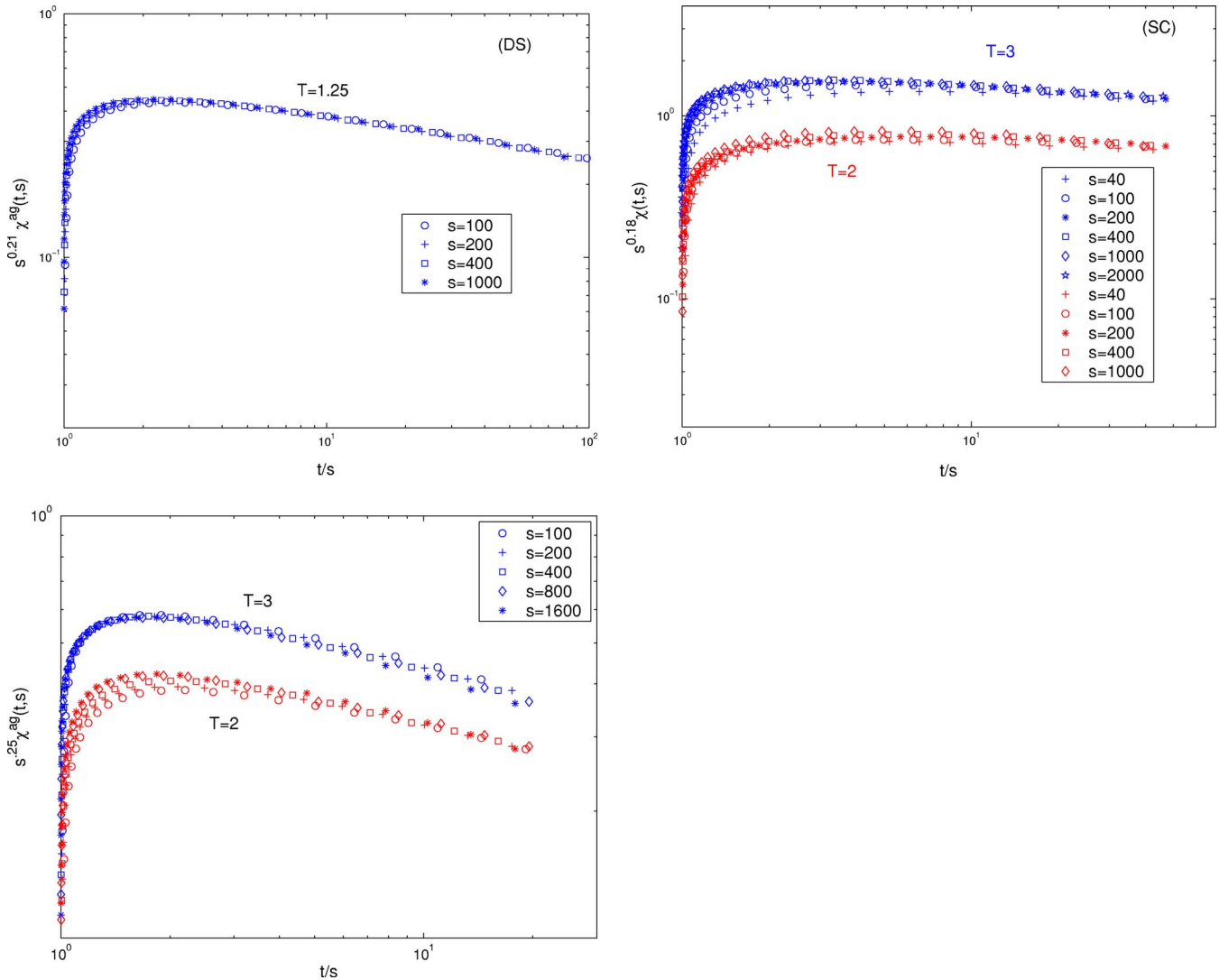


FIG. 17. (Color online) $\chi^{ag}(t,s)$ is plotted against $y=t/s$ for different values of s , at $T_f=1.25$ for the (DS), at $T_f=2$ and $T_f=3$ for the (TL) and the (SC).

overlaps $Q([\sigma], [\sigma']) = (1/N) \sum_i \sigma_i \sigma'_i$ between two configurations $[\sigma], [\sigma']$,

$$P_{eq}(q) = \frac{1}{Z} \sum_{[\sigma], [\sigma']} \exp\{-\beta(H[\sigma] + H[\sigma'])\} \times \delta(Q([\sigma], [\sigma']) - q). \quad (26)$$

Using the δ -like form of $P_{eq}(q)$ of the low temperature state of the ferromagnetic models considered in this paper, one obtains [23] the well-known broken line fluctuation-dissipation plot of χ versus C . However, as discussed in Ref. [6], when $a_\chi=0$ the theorem (25) cannot be applied straightforwardly and one gets a nontrivial fluctuation-dissipation plot which is not related to $P_{eq}(q)$.

V. DISCUSSION AND CONCLUSIONS

In this paper we have studied the phase-ordering kinetics of the Ising model with spin-flip dynamics on a class of

physical graphs. The evolution is in some respects qualitatively similar to what observed on regular lattices. After the quench one has the formation and growth of domains of the two competing ordered phases. Scaling symmetry is obeyed quite generally on finitely ramified structures, but not on infinitely ramified fractals in the range of times considered. Differently from coarsening on regular lattices, the fractal nature of the networks pins the interfaces on locally stable positions. Escape from the pinned positions is achieved by means of activated processes, but subsequently the interfaces are trapped again. When interfaces are pinned, the growth of the domain size $L(t)$ is inhibited. Because of this recurrent phenomenon the usual power growth law of $L(t)$ is modulated by an oscillation, which is more evident when the pinning is stronger, namely at low temperatures. The necessity of activated moves on many discrete time and/or space scales makes a great difference with respect to regular lattices. On regular lattices the temperature is an irrelevant parameter [1], in the sense of the renormalization group. Namely, in all the low temperature regions the dynamics is controlled by the

zero temperature fixed point. One has, therefore, the same dynamical exponents in all quenches to $T_f < T_c$, regardless of the temperature. On fractal networks, instead, the situation is different, because the dynamics of activated processes are faster the higher is T_f . As a consequence, exponents are always found temperature dependent.

A notable exception is the response function exponent a_χ , which turns out to be stable and temperature independent. This already suggests that a_χ may be related to a more fundamental property of the system which remains stable under temperature variations. Interestingly, we find $a_\chi = 0$ on all the considered graphs which do not support a ferroparamagnetic transition at a finite critical temperature, while $a_\chi > 0$ in all the other cases. The same situation was found [22–24] on regular lattices, where a_χ is related to the Euclidean dimension. On these lattices, the Euclidean dimension is the topo-

logical parameter that determines the existence of phase transitions and regulates the critical properties. This calls for the hypothesis that, also on generic graphs, a_χ could be related to the relevant topological features which govern the critical behavior, although for systems with a discrete symmetry, such as the Ising model considered here, a unique topological indicator, analogous to d is not known. For example, it is known that structures with the same fractal dimension and different lacunarity belongs to different universality classes [28]. Interestingly, our result suggests that a_χ can be used to infer topological properties of graphs.

ACKNOWLEDGMENT

This work has been partially supported from MURST through Grant No. PRIN-2004.

[1] A. J. Bray, *Adv. Phys.* **43**, 357 (1994).
 [2] H. Furukawa, *J. Phys. Soc. Jpn.* **58**, 216 (1989); *Phys. Rev. B* **40**, 2341 (1989).
 [3] D. A. Beysens, G. Forgacs, and J. A. Glazier, *Proc. Natl. Acad. Sci. U.S.A.* **97**, 9467 (2000); C. Castellano, M. Marsili, and A. Vespignani, *Phys. Rev. Lett.* **85**, 3536 (2000).
 [4] R. Burioni and D. Cassi, *J. Phys. A* **38**, R45 (2005).
 [5] Umberto Marini Bettolo Marconi and A. Petri, *Phys. Rev. E* **55**, 1311 (1997).
 [6] R. Burioni, D. Cassi, F. Corberi, and A. Vezzani, *Phys. Rev. Lett.* **96**, 235701 (2006).
 [7] U. Marini Bettolo Marconi, *Phys. Rev. E* **57**, 1290 (1998).
 [8] Y. Gefen, A. Aharony, and B. B. Mandelbrot, *J. Phys. A* **16**, 1267 (1983); Y. Gefen, A. Aharony, Y. Shapir, and B. B. Mandelbrot, *J. Phys. A* **17**, 435 (1984).
 [9] F. Corberi, E. Lippiello, and M. Zannetti, *Phys. Rev. E* **72**, 056103 (2005).
 [10] M. J. de Oliveira, J. F. F. Mendes, and M. A. Santos, *J. Phys. A* **26**, 2317 (1993). J. M. Drouffe and C. Godrèche, *ibid.* **32**, 249 (1999).
 [11] F. Liu and G. F. Mazenko, *Phys. Rev. B* **47**, 2866 (1993).
 [12] C. Chatelain, *J. Phys. A* **36**, 10739 (2003).
 [13] F. Ricci-Tersenghi, *Phys. Rev. E* **68**, 065104(R) (2003).
 [14] E. Lippiello, F. Corberi, and M. Zannetti, *Phys. Rev. E* **71**, 036104 (2005). Other methods for measuring the response function without applying the perturbation have been introduced in Refs. [12,13].
 [15] P. J. Grabner and W. Woess, *Stochastic Proc. Appl.* **69**, 127 (1997).
 [16] M. A. Bab, G. Fabricius, and E. V. Albano, *Phys. Rev. E* **71**, 036139 (2005).
 [17] D. Sornette, *Phys. Rep.* **279**, 239 (1998).
 [18] G. P. Zheng and M. Li, *Phys. Rev. E* **62**, 6253 (2000).
 [19] E. Lippiello and M. Zannetti, *Phys. Rev. E* **61**, 3369 (2000).
 [20] C. Godrèche and J. M. Luck, *J. Phys. A* **33**, 1151 (2000).
 [21] F. Corberi, C. Castellano, E. Lippiello, and M. Zannetti, *Phys. Rev. E* **70**, 017103 (2004).
 [22] F. Corberi, E. Lippiello, and M. Zannetti, *Phys. Rev. E* **65**, 046136 (2002).
 [23] F. Corberi, E. Lippiello, and M. Zannetti, *Phys. Rev. E* **63**, 061506 (2001); *Eur. Phys. J. B* **24**, 359 (2001).
 [24] F. Corberi, E. Lippiello, and M. Zannetti, *Phys. Rev. Lett.* **90**, 099601 (2003); *Phys. Rev. E* **68**, 046131 (2003).
 [25] R. Burioni, D. Cassi, and A. Vezzani, *Phys. Rev. E* **60**, 1500 (1999).
 [26] R. Burioni, D. Cassi, and C. Destri, *Phys. Rev. Lett.* **85**, 1496 (2000).
 [27] S. Franz, M. Mézard, G. Parisi, and L. Peliti, *Phys. Rev. Lett.* **81**, 1758 (1998); *J. Stat. Phys.* **97**, 459 (1999).
 [28] P. Monceau and P. Y. Hsiao, *Physica A* **331**, 1 (2004).